
Article:
Tickner, Benjamin, Rayner, Peter John orcid.org/0000-0002-6577-4117 and Duckett, Simon B. orcid.org/0000-0002-9788-6615 (2020) Using SABRE hyperpolarized ¹³C NMR to interrogate organic transformations of pyruvate. Analytical Chemistry. ac-2020-01334p.R1. pp. 1-9. ISSN 0003-2700

https://doi.org/10.1021/acs.analchem.0c01334

Using SABRE hyperpolarized ^{13}C NMR to interrogate organic transformations of pyruvate

Ben. J. Tickner, Peter J. Rayner, and Simon B. Duckett*

Center for Hyperpolarization in Magnetic Resonance (CHyM), Department of Chemistry, University of York, Heslington, York, YO10 5NY, U.K.

*simon.ducket@york.ac.uk

Supporting information Placeholder

ABSTRACT: Signal Amplification by Reversible Exchange (SABRE) is a hyperpolarization technique that uses a metal complex to catalytically transfer magnetization from *para*hydrogen to molecules of interest. SABRE is used here to monitor the decarboxylation of sodium pyruvate-1,2-[$^{13}C_2$] at a 15 mM concentration to form ethanoic acid and CO_2 upon reaction with hydrogen peroxide (150 mM). The rate constant of this reaction is determined by hyperpolarized ^{13}C SABRE-NMR as 0.056 ± 0.003 $dm^3\ mol^{-1}\ s^{-1}$ at 298 K and is comparable to that determined from thermal ^1H NMR (k = 0.050 ± 0.003 $dm^3\ mol^{-1}\ s^{-1}$) and UV measurements (k = 0.053 ± 0.001 $dm^3\ mol^{-1}\ s^{-1}$). The hyperpolarized reaction intermediate 2-hydroperoxy-2-hydroxypropanoate is detected in a single scan hyperpolarized ^{13}C NMR spectrum. This work highlights how SABRE hyperpolarization can be used as a tool for the precise monitoring of chemical transformations by hyperpolarized NMR spectroscopy.

Monitoring chemical change in real time gives insight into reaction mechanisms and subsequent yield optimizations. Many spectroscopic approaches have been developed to achieve this goal, such as IR and UV spectroscopy.[1] Nuclear Magnetic Resonance (NMR) spectroscopy is an alternative method, which uses non-ionizing radiation to study the magnetic environment of nuclei in a non-destructive manner. Despite this accomplishment, MR methods are relatively insensitive on a molecular level as the detected signal intensities are derived from small population perturbations between closely spaced nuclear spin energy levels. Consequently, at 9.4 T only 1 out of every 128,000 ^{13}C nuclei contribute positively to the MR signal detected for a ^{13}C enriched sample. This challenge often necessitates long experiment durations which limit both the ability of MR to detect species present at concentrations $< \mu M$ and the time scales over which chemical change can be accurately monitored.

Various hyperpolarization techniques are emerging which create non-Boltzmann derived population differences across these energy levels to address this sensitivity issue.[2] Of these, dissolution Dynamic Nuclear Polarization (d-DNP) has provided sufficient signal enhancement to enable the monitoring of chemical transformations such as Diels-Alder cycloadditions[3] or ligand complexation.[4] d-DNP also yields hyperpolarized probes suitable for monitoring metabolic transformations *in vivo*.[5] For example, the anaerobic conversion of hyperpolarized sodium pyruvate-1-[^{13}C] into products such as lactate and alanine can be used to identify cancer.[5,6]

An alternative method based on *para*hydrogen (p-H_2), a singlet spin isomer of dihydrogen, has also been developed. This approach began in the late 1980s with the detection of hydrogenation products[7,8] and has been termed *Para*Hydrogen Induced Polarization (PHIP).[9] The NMR signal gains PHIP provides have made the detection of low concentration catalytic intermediates[10-12] analytes,[13] and metabolites[9,14,15] by MR methods feasible. PHIP has provided mechanistic insight when p-H_2 is used to study hydrogenation reactions catalyzed by solid surfaces[16-18] or frustrated Lewis pairs.[19,20] However, a major limitation of PHIP is that it can only be applied to molecules containing unsaturated functionality. Over the last few decades, researchers have investigated new ways to introduce p-H_2 spin order into target molecules. One approach termed oneH-PHIP has been used to incorporate a single p-H_2 derived proton into an aldehyde.[21] This has allowed hydroformylation reactions to now be interrogated using p-H_2 and consequently, the enhanced NMR sensitivity has allowed detection of many intermediates in this process.[22]

In 2009, a non-hydrogenative variant of PHIP called Signal Amplification By Reversible Exchange (SABRE) was developed which does not require direct p-H_2 incorporation into the analyte.[23] Instead, the symmetry of p-H_2 is first broken by an oxidative addition reaction. Magnetization can then be transferred from the p-H_2 derived hydride ligands of the product to ligated substrates *via* the coupling network within the complex.[23,24] This process is catalytic in nature as p-H_2 and the substrate are both in reversible exchange. Therefore, the only requirement for hyperpolarization of a substrate using SABRE is the transient existence of a suitable metal catalyst.

This is usually achieved by the reaction of a stable SABRE precatalyst such as [IrCl(COD)(IMes)], (**1**) (where IMes = 1,3-*bis*(2,4,6-trimethyl-phenyl)imidazole-2-ylidene and COD = *cis*,*cis*-1,5-cyclooctadiene) with a substrate (sub) to form an active polarization transfer catalyst such as $[Ir(H)_2(IMes)(sub)_3]Cl$. Molecules containing *N*-donor sites that readily ligate to iridium such as *N*-heterocycles,[23,25,26] diazirines,[27-29] nitriles[30] and amines[31] are among the most

commonly reported examples of substrates that are hyperpolarized using SABRE.[32] Because of the matching conditions associated with the polarization transfer step involved in SABRE, it is usually performed at fields of around 6.5 mT for transfer into ^{1}H sites in the target,[23,25,26] while transfer to heteronuclei like ^{15}N and ^{13}C is achieved at μT fields.[33,34]

SABRE has the potential to allow *in situ* monitoring of a wider range of chemical transformations than PHIP. Some early examples include monitoring deuterium incorporation into the *ortho* sites of pyridine which occurs as a consequence of a hydrogen isotope exchange reaction.[35] Recently, the types of functional groups that SABRE can sensitize has been expanded by relayed proton exchange effects, termed SABRE-Relay. This has allowed the hyperpolarization of non-ligating molecules including alcohols, carboxylic acids, carbonates, phosphates, amides and silanols.[36-38] These effects have then been used to determine the rate of rapid reaction between *tris*(*tert*-butoxy)silanol and triflic anhydride.[38]

Hyperpolarized magnetization within target substrates decays back to its Boltzmann derived state according to a relaxation time constant, normally called T_1. Consequently, in order to monitor chemical change of hyperpolarized molecules, it is essential that the rate of transformation is faster than the rate of relaxation to allow for product to be created with retained non-Boltzmann magnetization. It is therefore clear that the following requirements must be met when selecting reactions suitable for monitoring using SABRE:

1. A reagent must be hyperpolarized with significant signal gains using SABRE.
2. A SABRE hyperpolarized reagent should contain a long lifetime to maximize the timescale over which chemical change can be monitored.
3. The chemical transformation should occur faster than relaxation to allow for the formation of product with hyperpolarized signal intensities.

SABRE has been used to create long lived p-H_2 derived singlet order within target substrates[27-29,39-41] (also called long lived singlet states) that now decay according to the time constant T_{LLS}, which is typically longer than T_1.[42] Consequently, the monitoring of reactions over longer timescales (of many minutes) may be feasible.

The strong substrate MR signals associated with hyperpolarization mean that reactions are often monitored by recording a series of single scan NMR spectra using low flip angle excitation.[3] The choice of flip angle is important as each excitation pulse consumes some of the available magnetization while the detection of small concentrations of product is favored by using a 90° flip angle. Low flip angles of between 5° and 15° are often a sensible balance point that allows reaction monitoring, whilst preventing signal loss before there is sufficient conversion to product. Therefore, the flip angle and time spacing between successive excitation pulses in addition to the nuclear spin relaxation rate and the reaction rate are important factors when deciding how best to examine a chemical transformation using hyperpolarized NMR.

We have recently reported the hyperpolarization of *O*-donor substrates such as sodium pyruvate-1,2-[$^{13}C_2$] using SABRE.[40] This was achieved by reacting a solution containing

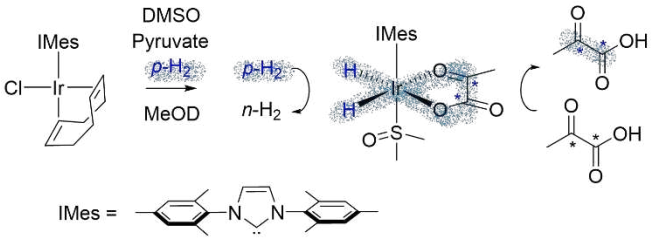

Figure 1: Hyperpolarization of sodium pyruvate-1,2-[$^{13}C_2$] by SABRE. Reaction of [IrCl(COD)(IMes)] with p-H_2, sodium pyruvate-1,2-[$^{13}C_2$], and DMSO yields the SABRE catalyst [Ir(H)$_2$(η^2-pyruvate)(IMes)(DMSO)]. Note that the asterisk (*) denotes a ^{13}C labelled position.

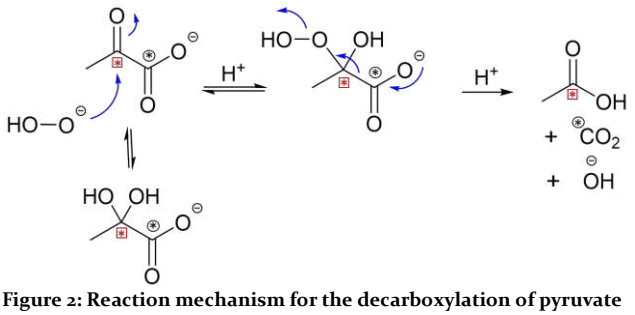

Figure 2: Reaction mechanism for the decarboxylation of pyruvate by hydrogen peroxide. This process involves the reversible attack of pyruvate by hydrogen peroxide, or the peroxide anion, to form a tetrahedral 2-hydroperoxy-2-hydroxypropanoate intermediate which decarboxylates to form ethanoic acid and carbon dioxide. Note that the asterisk (*) denotes a ^{13}C labelled position.

[IrCl(COD)(IMes)] (**1**, 5 mM), DMSO (8 eq.), and sodium pyruvate-1,2-[$^{13}C_2$] (6 eq.) with 3 bar H_2 in methanol-d_4 (0.6 mL) to form [Ir(H)$_2$(η^2-pyruvate)(IMes)(DMSO)] (**2**) as depicted in Figure 1.[40,43] Upon shaking these solutions with 3 bar p-H_2 at the μT fields necessary to transfer magnetization directly from p-H_2 derived hydride ligands to ligated ^{13}C pyruvate sites, ^{13}C NMR signal enhancements of ~ 1000 fold are readily achieved.[44] Interestingly, SABRE can be used to prepare hyperpolarized pyruvate-[$^{13}C_2$] in a long lived nuclear spin state with a T_{LLS} of ~43 s at high field (11.7 T) which exceeds the T_1 times of the individual spins (~34 s and ~21 s for its $^{13}C_1$ and $^{13}C_2$ sites respectively).[40]

In this paper we show that the ^{13}C pyruvate signal gains achieved using SABRE are sufficient in both magnitude and lifetime to allow the monitoring of rapid chemical transformations. We do this by using SABRE to monitor the reaction between hyperpolarized sodium pyruvate-1,2-[$^{13}C_2$] and hydrogen peroxide (H_2O_2) to form ethanoic acid and carbon dioxide. This reaction begins with nucleophilic attack of peroxide on the keto-group of pyruvate to give 2-hydroperoxy-2-hydroxypropanoate which readily decarboxylates under acidic conditions, as shown in Figure 2.[45-47] The rate of this reaction is dependent on pH and carbon kinetic isotope effects which suggest that as the pH is increased the rate determining step changes from formation of the tetrahedral intermediate to its decarboxylation.[47] The associated 2-hydroperoxy-2-hydroxypropanoate intermediate is unstable and too short lived to be observed by typical spectroscopic analyses at room temperature.[45] Nevertheless, it has been observed by NMR when the reaction between sodium pyruvate-1-[^{13}C] or sodium pyruvate-2-[^{13}C] and H_2O_2 is performed at low temperature (238-259 K).[45] Here, we use the NMR signal gains SABRE can deliver to make this intermediate visible in a single scan ^{13}C NMR spectrum at

298 K. We also examine the condensation reaction that takes place between sodium pyruvate and an amine that proceeds over a longer timescale[48] and demonstrate that it is too slow to follow by this approach.[39] In doing so, we produce results that allow us to discuss the feasibility of using SABRE to monitor reactions in which reactants or products coordinate to the SABRE catalyst.

EXPERIMENTAL SECTION

Materials All commercial compounds were purchased from Sigma-Aldrich and used as supplied. The SABRE precatalyst [IrCl(COD)(IMes)] was synthesized according to literature procedures.[49] *Para*-hydrogen (*p*-H_2) with *ca.* 99% purity[50] was produced by passing hydrogen gas over a spin-exchange catalyst (Fe_2O_3) at 28 K.

Equipment NMR measurements were carried out on a 400 MHz Bruker Avance III spectrometer using solutions at room temperature unless otherwise stated. ^{1}H (400 MHz) and ^{13}C (100.6 MHz) NMR spectra were recorded with an internal deuterium lock. ^{13}C NMR spectra were recorded with broadband proton decoupling. Chemical shifts (δ) are quoted as parts per million and referenced to methanol-d_4 solvent. UV spectra were collected using a Thermoscientific evolution array UV-vis spectrophotometer.

Reaction of sodium pyruvate with H_2O_2 by ^{1}H NMR spectroscopy. A solution of 300 mM H_2O_2 in D_2O (300 μL) (9.6 μL of a 30% w/w H_2O_2 in H_2O solution in 290.4 μL D_2O) was added to sodium pyruvate (30 mM) in 4:96 methanol:methanol-d_4 (300 μL) in a J. Young's fitted NMR tube at 298 K. A series of 90° single scan ^{1}H NMR spectra, at 25 second time intervals, were recorded immediately after the sample was shaken for ~1 second in the Earth's field to aid mixing. The integral intensities of the ^{1}H CH_3 resonances of pyruvate (A), pyruvate hydrate (B) and ethanoic acid (C) were converted to concentration and then plotted over time. This data was fitted to a kinetic model to extract the rate of reaction between pyruvate and H_2O_2 (D). The model is depicted in Scheme 1 and described by Equations 1-4 where $\boldsymbol{\delta t}$ is an incremental time difference and $k_{H_2O_2}$, k_{Hy} and k_{-Hy} are the rates of reaction between pyruvate and H_2O_2, formation of pyruvate hydrate from pyruvate, and formation of pyruvate from its hydrate respectively. Species such as H_2O, pyruvate dimers, or enol pyruvate were omitted as they were either in excess or not observed in these measurements. A pathway that allows for reaction of pyruvate hydrate with H_2O_2 was not included as it has been previously reported to be slow.[45]

$$\mathrm{B} \underset{k_{Hy}}{\overset{k_{-Hy}}{\rightleftharpoons}} \mathrm{A} \xrightarrow[+\,H_2O_2]{k_{H2O2}} \mathrm{C}$$

Scheme 1: Model used to fit the reaction between sodium pyruvate and H_2O_2

$$[A]_{t+\delta t} = [A]_t + \left(-k_{H2O2}[A]_t[D]_t - k_{Hy}[A]_t + k_{-Hy}[B]_t\right)\partial t \quad (1)$$

$$[B]_{t+\delta t} = [B]_t + \left(k_{Hy}[A]_t - k_{-Hy}[B]_t\right)\partial t \quad (2)$$

$$[C]_{t+\delta t} = [C]_t + \left(k_{H2O2}[A]_t[D]_t\right)\partial t \quad (3)$$

$$[D]_{t+\delta t} = [D]_t - \left(k_{H2O2}[A]_t[D]_t\right)\partial t \quad (4)$$

Rate constants were found by minimizing the differences between experimentally determined concentrations and calculated values. The model was constrained to set the predicted initial concentrations of each reagent to within 10% of those experimentally determined from the first ^{1}H NMR spectrum.

Monitoring H_2O_2 reaction with pyruvate by UV spectroscopy. A series of UV spectra, separated by 5 second time intervals, were recorded following the addition of 32 μL H_2O_2 (30% w/w H_2O_2 in H_2O solution, final H_2O_2 concentration of 150 mM) to sodium pyruvate (15 mM) in 51:49 methanol:H_2O (1.97 mL). The resulting absorbances at λ_{max} were baseline corrected and fitted to the kinetic model described by equations 1-4.

Production of hyperpolarized pyruvate using SABRE Solutions of hyperpolarized sodium pyruvate-1,2-[$^{13}C_2$] are produced by preparing samples containing [IrCl(COD)(IMes)] (3 mM), DMSO (8 eq.), and sodium pyruvate-1,2-[$^{13}C_2$] (6 eq.) in 288 μL methanol-d_4 and 12 μL methanol in a 5 mm NMR tube fitted with a J. Young's tap. The solutions were subsequently degassed by two freeze-pump-thaw cycles and were activated with 3 bar H_2 and left at room temperature for 30 mins to allow the formation of [Ir(H)$_2$(η^2-pyruvate)(IMes)(DMSO)] as confirmed by ^{1}H NMR spectroscopy.[40,43] Subsequently, the sample was shaken with fresh *p*-H_2 (3 bar) for 30 seconds in a mu metal shield (*ca.* 300-fold shielding) at room temperature to produce SABRE hyperpolarized pyruvate. This has been described in more detail elsewhere.[40,43,44]

Monitoring H_2O_2 reaction with pyruvate hyperpolarized using SABRE. Immediately after *p*-H_2 shaking solutions of **2**, the J. Young's valve was removed from the NMR tube whilst leaving the sample in the mu metal shield. A solution of H_2O_2 (9.6 μL of a 30% w/w solution in H_2O) in D_2O (290.4 μL) was added to give a final H_2O_2 concentration of 150 mM. The valve was replaced and the sample shaken for ~1 second in the shield to mix the solution at room temperature before rapidly inserting into the 9.4 T spectrometer for NMR monitoring. This involved the collection of a succession of single scan 10° ^{13}C NMR spectra at 298 K separated by 6 second time intervals up to a 120 second reaction time. The integral intensities of the [1-^{13}C] resonance of pyruvate (A), and CO_2 (E), or the pyruvate [2-^{13}C] site (A) and ethanoic acid (C) were analyzed according to a kinetic model. In this model the hyperpolarized signals of species X, S_X detected by the 10° pulse at time t is calculated according to equation 5 where M_X is the magnetization of species X and θ is the flip angle. The magnetization of species X remaining after the pulse is given by equation 6.

$$(S_X)_t = (M_X)_{t-\delta t}\sin\theta \quad (5)$$

$$(M_X)_t = (M_X)_{t-\delta t}\cos\theta \quad (6)$$

The magnetization of pyruvate (A) and CO_2 (E) or ethanoic acid (C) change during the time interval between pulses due to chemical reaction and relaxation according to equations 7 and 8 where T_A and $T_{C,E}$ are the relaxation times of the ^{13}C resonances of pyruvate, CO_2 or ethanoic acid respectively and k is a pseudo first order rate constant described in Equation 9.

$$(M_A)_{t+\delta t} = (M_A)_t + \left(-k(M_A)_t - \frac{(M_A)_t}{T_A}\right)\delta t \quad (7)$$

$$\left(M_{C,E}\right)_{t+\delta t} = \left(M_{C,E}\right)_t + \left(k\left(M_{C,E}\right)_t - \frac{\left(M_{C,E}\right)_t}{T_{C,E}}\right)\delta t \qquad (8)$$

$$k_{H2O2} = k[D] \qquad (9)$$

Bound pyruvate, pyruvate hydrate and HCO_3^- (which often exists in equilibrium with CO_2,[45] particularly in living systems)[5] were excluded from this model as no hyperpolarized signals for these species were visible, or in the case of HCO_3^-, its hyperpolarized integral intensities were < ~3% of all the hyperpolarized ^{13}C NMR signals. Rate constants were then determined as described previously. Relaxation times of these species were not fixed and fitted parameters are given in the supporting information.

Monitoring the reaction between pyruvate and amine by NMR. A succession of single scan ^{13}C NMR spectra, acquired with 10° pulses, were recorded after the addition of phenylethylamine (PEA) (26.5 mM) to SABRE hyperpolarized sodium pyruvate-1,2-[$^{13}C_2$] (30 mM) in methanol-d_4 (0.6 mL). This reaction was also monitored by thermally polarized ^1H NMR measurements at 298 K and a reaction rate constant extracted using a similar model to that described by equations 1-4 (see supporting information.).

RESULTS AND DISCUSSION

Monitoring the reaction of sodium pyruvate with H_2O_2 by ^1H NMR

A solution of sodium pyruvate (15 mM) and hydrogen peroxide (150 mM) in D_2O was monitored using ^1H NMR spectroscopy at 9.4 T. This involved recording a series of single scan spectra using a 90° flip angle that were separated by 25 second intervals in order to ensure a quantitative response. This time interval was chosen as ^1H T_1 measurements on separate 15 mM solutions of sodium pyruvate and ethanoic acid in the proportion 48:2:48:2 D_2O:H_2O:CD_3OD:CH_3OH yielded values of 5.7 s and 4.0 s for their CH_3 protons at 9.4 T. When the first ^1H NMR spectrum of this series is examined, ^1H NMR resonances corresponding to the CH_3 group of pyruvate at δ 2.35 and its hydrate at δ 1.45 are observed. No signals for pyruvate hemiacetal were observed in these measurements. Weaker signals appear for the methyl and carboxylate protons of ethanoic acid at δ 1.94 and 10.99 respectively. Representative spectra are given in the supporting information.. As the reaction proceeds, the resonances corresponding to pyruvate, and its hydrate, decrease in intensity while those of ethanoic acid increase. These signal intensity changes are proportional to concentration and fit to a kinetic model

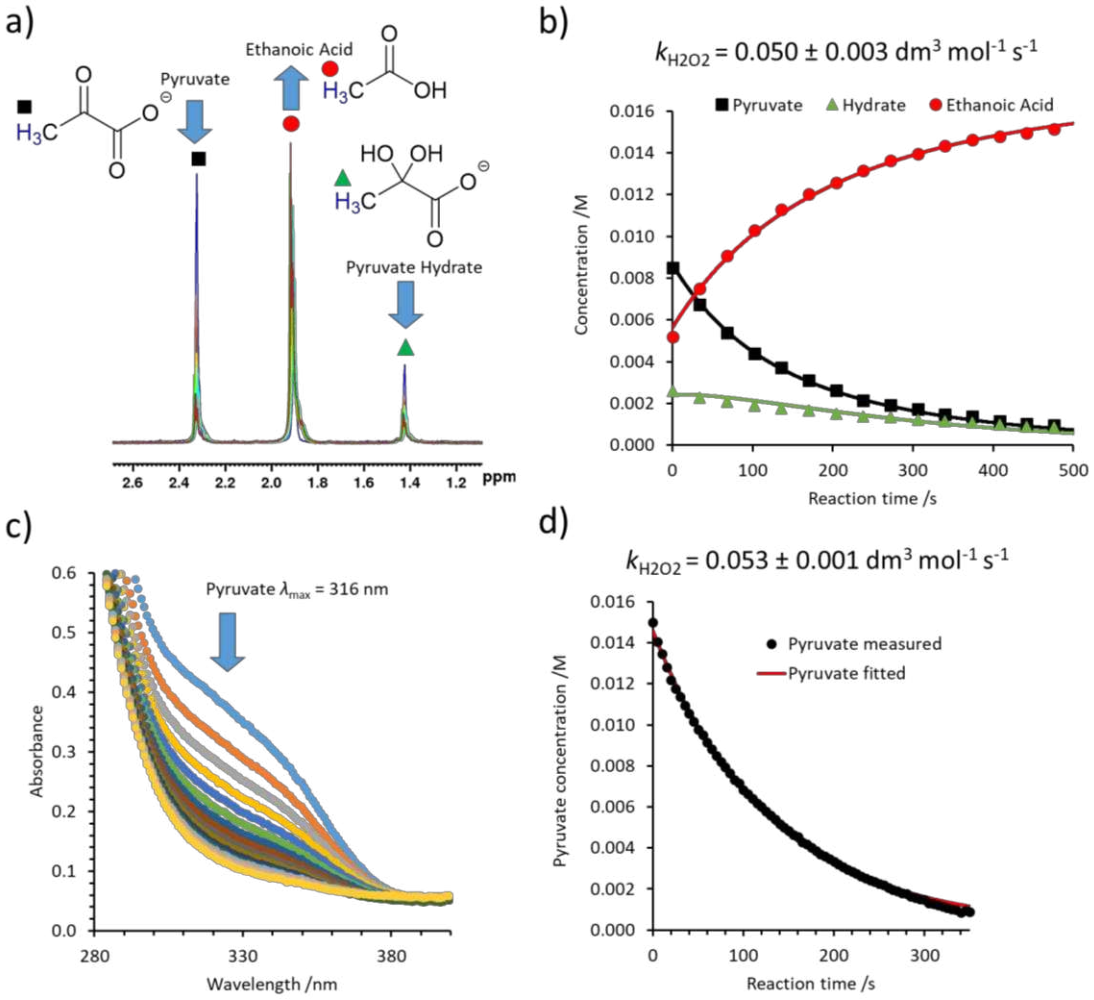

Figure 3: a) A series of partial 90° ^1H NMR spectra of a solution of sodium pyruvate (30 mM) in 4%:96% methanol:methanol-d_4 (300 μL) recorded at 25 second time intervals after the addition of 300 mM H_2O_2 in D_2O (300 μL) to illustrate reaction progress b) Kinetic fitting of this NMR data c) partial UV absorption spectra of an analogous solution of sodium pyruvate (15 mM) in 51:49 methanol:H_2O (1.968 mL) (top, blue) where example UV traces are recorded every 30 seconds after the addition of 32 μL H_2O_2 (30% w/w H_2O_2 in H_2O solution, final H_2O_2 concentration of 150 mM) d) associated kinetic fitting of this UV data with extracted rate constant.

(described in the experimental) in order to obtain the effective reaction rate constant, $k_{H_2O_2}$, of 0.050 ± 0.003 $dm^3\ mol^{-1}\ s^{-1}$ (see supporting information.). $k_{H_2O_2}$ determined by UV measurements has been reported to vary between 0.1 and 1 $dm^3\ mol^{-1}\ s^{-1}$ depending on the pH of the buffered reaction mixture.[46] However, these rates are from studies with more dilute reagent concentrations (1.5 mM pyruvate and 5-30 mM H_2O_2). $k_{H_2O_2}$ has also been determined using ^{13}C NMR spectroscopy at much lower temperatures (238-259 K).[45] From these data $k_{H_2O_2}$ at 298 K is predicted to be ~0.16 $dm^3\ mol^{-1}\ s^{-1}$. Therefore, $k_{H_2O_2}$ calculated from our ^1H NMR measurements is slower than that predicted by a factor of three. Inefficient sample mixing or differences in solvent composition may account for this. Analogous measurements using ^{13}C NMR spectroscopy could not be recorded here as the signal strengths are not sufficient to detect a signal in the necessary time period, even with signal averaging.

These experiments were then repeated in the presence of the SABRE catalyst [Ir(H)$_2$(η^2-pyruvate)(IMes)(DMSO)], (**2**, 3 mM) to determine if the presence of the metal complex influences the rate of reaction between pyruvate and H_2O_2. In these cases, the kinetic time course from analogous ^1H NMR measurements no longer fit the model described in the experimental (see supporting information). This is perhaps unsurprising as additional reaction pathways, which include reversible ligation of pyruvate to the metal catalyst, can occur. The chemical shift of the pyruvate CH_3 signal when bound in **2** has been reported, although it overlaps with signals of the IMes ligand.[40] The influence of the metal on this reaction can, however, be negated by adding a chelating ligand such as phenanthroline to destroy **2** before the addition of H_2O_2.[51] When the corresponding kinetic data are collected following the addition of H_2O_2 to a solution of **2** deactivated with phenanthroline (5 eq.), $k_{H_2O_2}$ was found to be 0.051 ± 0.003 $dm^3\ mol^{-1}\ s^{-1}$. This value is therefore consistent with that determined from solutions without **2** (0.050 ± 0.003 $dm^3\ mol^{-1}\ s^{-1}$) thereby establishing that the presence of the metal complex influences the reaction and can be suppressed if it is first deactivated by phenanthroline addition.

Monitoring the reaction of sodium pyruvate with H_2O_2 by UV spectroscopy

The rate of reaction between sodium pyruvate and hydrogen peroxide was also determined using ultraviolet (UV) spectroscopy. A UV spectrum of sodium pyruvate (15 mM) in 51:49 methanol:H_2O (1.97 mL) revealed a λ_{max} of 316 nm which compares well to previously reported values of 316 nm,[52] 325 nm[53] and 326 nm.[54] This involved recording a series of UV spectra at 5 second time intervals after the addition of H_2O_2 (150 mM). The decrease in λ_{max} at 316 nm was fitted to the kinetic model described by equations 1-4 (see experimental). As a control, no significant change in λ_{max} was observed when solutions were monitored in the absence of H_2O_2. Furthermore, photolysis of pyruvate is known to cause UV induced $\pi \rightarrow \pi^*$ transitions in the pyruvate keto-group which leads to the formation of a range of products, including lactic acid, dimethyltartaric acid and acetoin.[54] None of these photolysis products were detected by NMR or MS which is consistent with the shorter UV irradiation times in these kinetic measurements (< 5 minutes) compared to the photolysis studies (~1 hour).[54] $k_{H_2O_2}$ was subsequently determined to be 0.053 ± 0.001 $dm^3\ mol^{-1}\ s^{-1}$ (by UV spectroscopy) which is consistent with the value determined by ^1H NMR spectroscopy. The effect the SABRE catalyst has on this reaction could not be investigated by UV spectroscopy as its presence masked UV absorption by pyruvate (see supporting information).

Monitoring the reaction of sodium pyruvate and H_2O_2 using SABRE hyperpolarized NMR

The rate of reaction between sodium pyruvate and hydrogen peroxide was then measured using SABRE hyperpolarized ^{13}C NMR spectroscopy. Sodium pyruvate, with ^{13}C labels in both the carboxyl and keto positions, was used as the reagent because the presence of these two ^{13}C labels results in the creation of singlet spin order by SABRE which has a longer lifetime than the more usual single spin (Zeeman) order associated with NMR.[40] Consequently, its use should facilitate the observation of chemical change occurring over a longer time window than would otherwise be possible. A further benefit is that the chemical fate of both sites can be followed in a single experiment.

The required SABRE hyperpolarized pyruvate (15 mM) was produced by shaking **2** with 3 bar p-H_2 in a mu-metal shield for 30 seconds before H_2O_2 was added (final concentration of 150 mM) and the sample was inserted into a 9.4 T spectrometer at 298 K. A series of time separated single scan ^{13}C measurements were then recorded with 10° flip angles. Insertion into the magnet will convert the initial $^{13}C_2$ singlet state created during SABRE into both longitudinal two and single spin order terms which both contribute to the detected signal intensity.[40,43,44] The former does so in the form of an antiphase doublet while the latter leads to in-phase doublets of opposite relative phase at the two sites.[40]

Hyperpolarized ^{13}C NMR signals for free pyruvate (δ 170 and 202) and pyruvate bound within **2** (δ 169 and 205) are observed with both these features in the early ^{13}C NMR spectra. Hyperpolarized resonances are also readily observed for the reaction products ethanoic acid and CO_2 at δ 182 and 122 respectively in these NMR spectra (see supporting information).As expected, the two pyruvate ^{13}C NMR signals decrease in intensity over time, while those of the reaction products first increase as they build-up and then fall as the effects of relaxation begin to dominate. When such a sample was removed from the spectrometer and shaken with fresh p-H_2 no hyperpolarized signals were visible; at this time point reaction between pyruvate and H_2O_2 is complete. It is therefore clear that SABRE is able to monitor this change, a feat that is not possible using the usual Boltzmann derived ^{13}C Zeeman polarization due to low sensitivity and the need for signal averaging.

A kinetic rate constant for this chemical change can be derived from these data. However, kinetic modelling must now account for both reactivity, signal relaxation, and the magnetization reduction associated with the successive 10° pulses. We have shown earlier how **2** can affect this process and therefore we negate its effect by addition of phenanthroline (Figure 4). Both pyruvate [1-^{13}C] and [2-^{13}C] sites should receive the same initial hyperpolarisation as

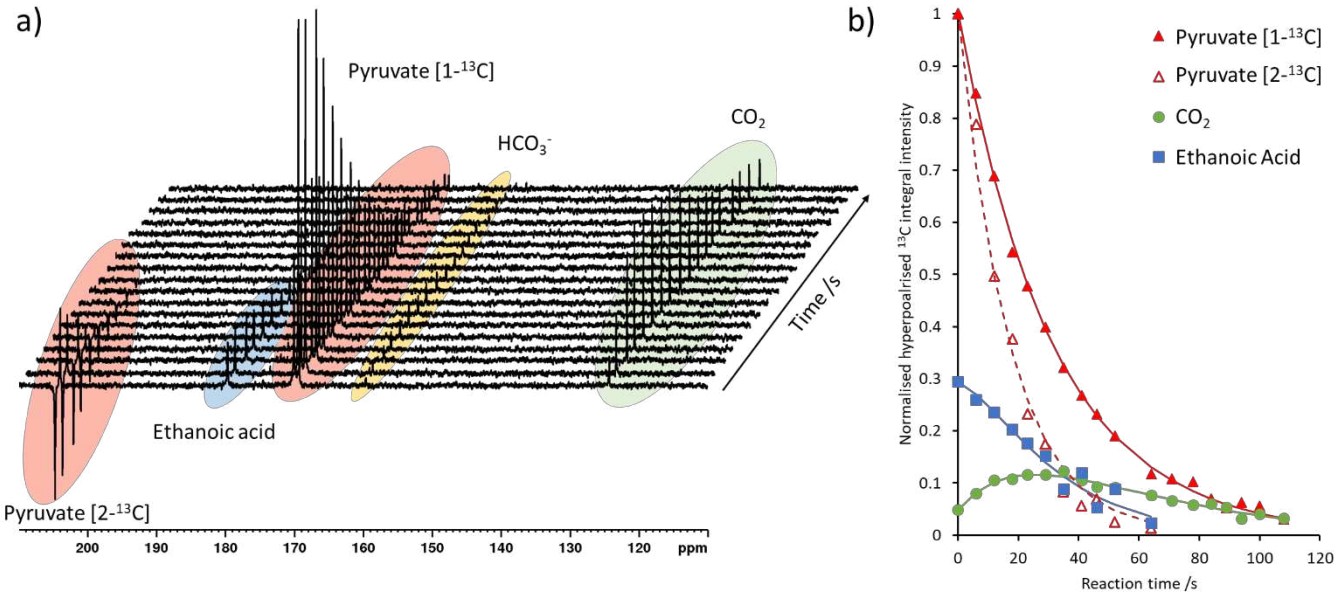

Figure 4: a) A series of partial 10° single scan ^{13}C NMR spectra recorded after the addition of 150 mM H_2O_2 and phenanthroline (5 eq. relative to 2) to a solution of SABRE hyperpolarized sodium pyruvate-1,2-[$^{13}C_2$] (15 mM) in methanol-d_4 (0.6 mL) at 298 K b) Associated changes in hyperpolarized signal intensity over reaction time can be plotted (marker points) and are fit to the kinetic model described by equations 5-9 (solid lines). The fitting parameters are given in the supporting information.

magnetisation is shared equally across the two coupled ^{13}C sites of the singlet state.[40,44] However, the shorter reported T_1 time of the [2-^{13}C] site (~21 s compared to ~34 s for the [1-^{13}C] site [40] results in a lower signal intensity for this site at longer measurement time. This is evident in spectra shown in Figure 4a which are recorded 10-15 seconds after initial preparation of the hyperpolarized $^{13}C_2$ state due to the time taken to add phenanthroline and H_2O_2. The contribution from the two spin order terms was removed by taking the sum of the two individual peaks involved in each multiplet for each pyruvate ^{13}C signal. Upon fitting this data using the model described by equations 5-9 of the experimental to the [1-^{13}C] pyruvate signal, a k_{H2O2} value of 0.056 ± 0.003 dm^3 mol^{-1} s^{-1} was obtained which is consistent with the value obtained from the corresponding thermal ^1H NMR measurements (k_{H2O2} = 0.050 ± 0.003 dm^3 mol^{-1} s^{-1}).

When the [2-^{13}C] pyruvate signal and the ethanoic acid signal are analyzed, the corresponding k_{H2O2} value proved to be 0.055 ± 0.040 dm^3 mol^{-1} s^{-1}. The higher uncertainty of this value stems from the shorter T_1 of the [2-^{13}C] pyruvate site (model fitted values of 20.6 ± 3.7 s compared to 47.3 ± 1.2 s for the [1-^{13}C] site) which reduces the time scale over which the reaction can be followed (to ~40 s rather than ~90 s for the [1-^{13}C] site). These thermal and hyperpolarized NMR measurements were repeated at a final H_2O_2 concentration of 100 mM and yielded comparable values of k_{H2O2} (0.051 ± 0.003 dm^3 mol^{-1} s^{-1} compared to 0.045 ± 0.001 dm^3 mol^{-1} s^{-1} from thermal NMR, see supporting information).

SABRE makes the short lived 2-hydroperoxy-2-hydroxypropanoate intermediate visible in single scan ^{13}C NMR

The reaction between sodium pyruvate and H_2O_2 occurs *via* the tetrahedral 2-hydroxperoxy-2-hydroxypropanoate intermediate of Figure 2.[47] [45,46] ^{13}C NMR signals for this intermediate have previously been reported at δ 102.9 and 178.3 in conjunction with a low temperature (238-259 K) study.[45] Closely related ethyl 2-hydroxperoxy-2-hydroxypropanoate, formed from the analogous reaction with ethyl pyruvate, has also been observed by ^{13}C and ^1H NMR at 298 K.[46] In the SABRE NMR measurements just described, we failed to observe ^1H or ^{13}C NMR signals for this species at 298 K. However, this species was detected in a single scan ^{13}C NMR spectrum at 260 K with a 90° read pulse when this study was repeated by adding H_2O_2 to

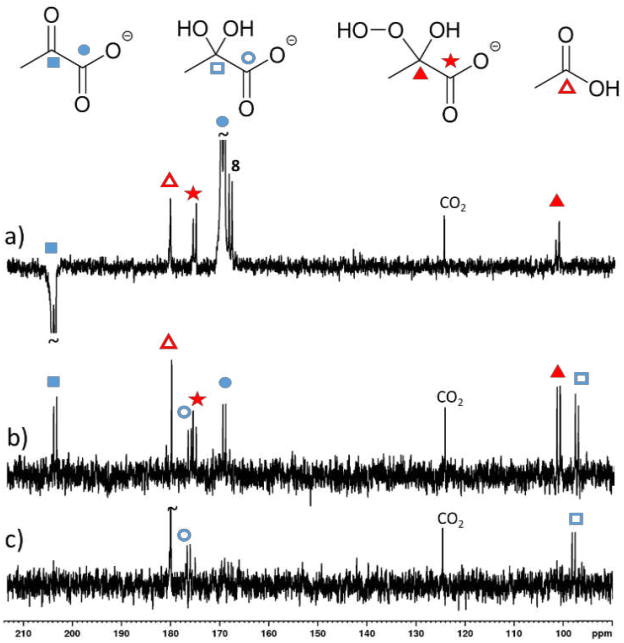

Figure 5: a) A single scan hyperpolarized ^{13}C NMR spectrum recorded with a 90° flip angle immediately after the addition of H_2O_2 (final H_2O_2 concentration of 150 mM) at ~ 195 K to a solution containing hyperpolarized sodium pyruvate-1,2-[$^{13}C_2$] b) and c) are 128 scan ^{13}C NMR spectra recorded under Boltzmann conditions at 260 K roughly b) 4 minutes and c) 10 minutes after initial H_2O_2 addition. Note that a) has been expanded vertically by a factor of 4 relative to b) and c). The spectrometer was set to 260 K in these experiments, although in a) the solution temperature is likely to be lower as the temperature equilibrates.

hyperpolarized sodium pyruvate-1,2-[$^{13}C_2$] at ~195 K. ^{13}C NMR signals for 2-hydroperoxy-2-hydroxypropanoate appear at δ 101.7 and 175.8 ($^{1}J_{CC}$ = 65 Hz), as shown in Figure 5, and compare well with previously reported values.[45,46] Signals for pyruvate, pyruvate bound in **62a**, ethanoic acid and CO_2 are also visible in addition to a species at δ 97.94 and 176.68 which we assign as pyruvate hydrate, though could be consistent with pyruvate hemiacetal.[45] Signals for this intermediate can also be observed in a single scan when the spectrometer is set to 273 K (see supporting information). We conclude the lifetime of this species must be too short to allow detection at 298 K under the conditions reported here.

SABRE hyperpolarized sodium pyruvate to study organic transformations

α-Keto acids such as pyruvate exhibit a diverse range of chemical reactivity being well known to form imines *via* transamination reactions with amines.[48] This reaction is usually slow and can be facilitated by an enzyme and pyridoxal cofactor, although it can also be promoted by transition metal complexes.[39] SABRE hyperpolarized NMR was therefore used to see if it could provide a way to follow such imine formation. A succession of single scan ^{13}C NMR spectra recorded with 10° pulses were recorded after the addition of phenylethylamine (PEA) (26.5 mM) to SABRE hyperpolarized sodium pyruvate-1,2-[$^{13}C_2$] (30 mM) in methanol-d_4 (0.6 mL). Unfortunately, while enhanced ^{13}C NMR signals were seen for free pyruvate, pyruvate hydrate, and **2**, (see supporting information) these signals decreased in intensity with increase in reaction time and no signals for additional species were observed. Hence, neither the hemiaminal intermediate nor the imine product were observed over the ~60 second observation window afforded by the hyperpolarized response.

When this experiment was repeated using a series of 64 scan thermally polarized ^{1}H NMR measurements to encode the reaction, signals corresponding to **2** at δ – 27.08 and – 29.01 were immediately replaced by those of two new complexes that yield hydride signals at δ – 22.44 and – 22.48. The species giving rise to these signals are [Ir(H)$_2$(IMes)(PEA)$_3$]Cl, **3** and [Ir(H)$_2$(IMes)(DMSO)(PEA)$_2$]Cl, **4** as reported previously.[31,37] Unfortunately, these species form rapidly as a result of the reaction of **2** with added amine.[44,55] As the reaction time is extended, additional sets of hydride signals appear at δ –21.52, –28.50 and δ –21.00, –26.20. These products are identified as [Ir(H)$_2$(η^2-α-carboxyimine)(PEA)(IMes)], **5** and [Ir(H)$_2$(η^2-α-carboxyimine)(DMSO)(IMes)], **6**[39,55] of Figure 6 and result from the expected pyruvate condensation. Eventually, **6** dominates these ^{1}H NMR spectra and 2D NMR characterization at 245 K confirms this assignment (see supporting information). We associate the inability of hyperpolarized NMR to follow the reaction between pyruvate and amine to be the result of the slow reaction rate when compared to T_1. Tests to increase the reaction rate by increasing the phenethylamine concentration to 150 mM in conjunction with a 15 mM sodium pyruvate-1,2-[$^{13}C_2$] concentration were also unsuccessful (see supporting information). However, the corresponding thermal ^{1}H NMR spectroscopy measurements now yielded a reaction rate constant, k, of 0.017 ± 0.001 dm^3 mol^{-1} s^{-1} (see supporting information). This reaction is therefore *c.a.* three times slower than that with H_2O_2 which is consistent with the failure to monitor this reaction using SABRE enhanced NMR.

CONCLUSIONS

We show here that SABRE hyperpolarized ^{13}C NMR can be used to monitor the rapid chemical transformation of sodium

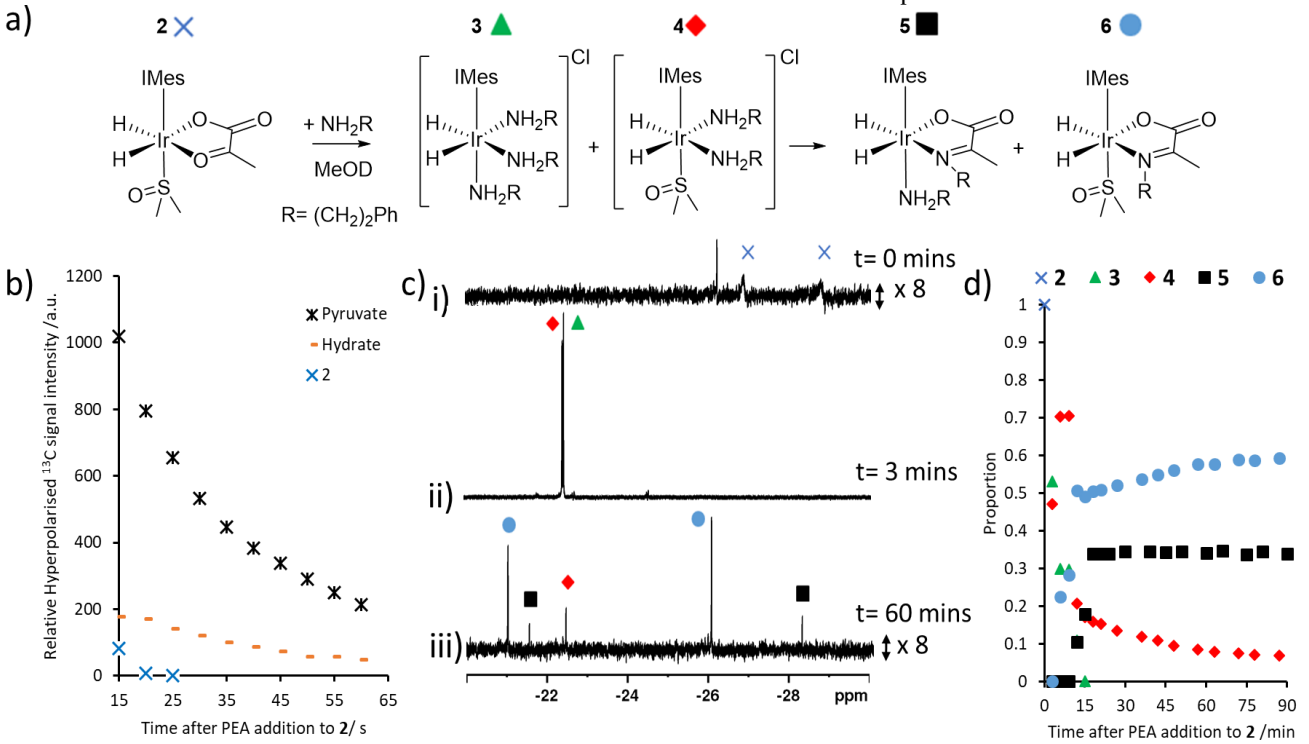

Figure 6: a) Summary of chemical changes that occur upon addition of phenethylamine to 2 b) Change in relative hyperpolarized ^{13}C signal intensity of pyruvate, bound pyruvate and pyruvate hydrate as determined by recording a series of ^{13}C NMR spectra with 10° flip angles. c) representative ^{1}H NMR spectra of the hydride region and d) associated time course data as determined from a series of 32 scan ^{1}H NMR measurements when PEA (5 eq.) is added to 2 in methanol-d_4 (0.6 mL) at 298 K.

pyruvate-1,2-[$^{13}C_2$] into CO_2 and ethanoic acid. Quantification of the SABRE response allowed the successful monitoring of this reaction *via* [1-^{13}C] and [2-^{13}C] pyruvate ^{13}C NMR signals, the former having the longest T_1. Analysis of the time dependent intensities of these signals, following removal of the effects of relaxation, led to a rate constant of 0.056 ± 0.003 dm^3 mol^{-1} s^{-1} for this reaction at 298 K. This rate constant is consistent with those determined from analogous ^{1}H NMR and UV control measurements (0.050 ± 0.003 dm^3 mol^{-1} s^{-1} and 0.053 ± 0.001 dm^3 mol^{-1} s^{-1} respectively) thereby establishing the validity of the method. The presence of the iridium SABRE catalyst was shown to influence the rate of this transformation, but its effect was removed once it was deactivated by the addition of phenanthroline. This reaction involves the intermediate 2-hydroxperoxy-2-hydroxypropanoate which is too short lived to be detected by NMR spectroscopy at 298 K, however, the ^{13}C NMR signal gains arising from SABRE enabled its observation in a single-scan ^{13}C NMR measurement at reduced temperature.

Attempts were also made to monitor the conversion of pyruvate into an imine by reaction with phenethylamine. Unfortunately, this reaction was too slow to follow by SABRE enhanced NMR, although a rate constant of 0.017 ± 0.001 dm^3 mol^{-1} s^{-1} could be estimated by ^{1}H NMR spectroscopy. Normally, as SABRE is reversible it can continually re-hyperpolarize molecules (unlike DNP and PHIP in which hyperpolarization is created in a batch process). Hence, there is the potential to monitor concentration changes over longer timescales by simply repeating the SABRE process. Sadly, this option was not possible here as the addition of phenethylamine to the SABRE hyperpolarized pyruvate solution leads to destruction of **2** which prevents the re-hyperpolarization of pyruvate.

In conclusion, we have demonstrated in this work how SABRE enhanced NMR can be used to follow a reaction and produce accurate reaction rate data whilst detecting a short-lived reaction intermediate. SABRE has been applied to hyperpolarize a growing range of substrates with diverse chemical reactivity,[32] some of these have been created as long lived $^{15}N_2$ singlet states[27-29] and others have been prepared with significant longitudinal magnetic lifetimes.[25,41,56] Therefore, it is likely that the benefits of the simple analytical route presented in this work will be applicable to the study of chemical reactivity and reaction kinetics of a wider range of chemical systems. Recent work showing that low-field NMR measurements are possible in conjunction with hyperpolarization have firmly demonstrated that low MR sensitivity can be addressed.[35,57-59] Both singlet state lifetimes, and indeed relaxation times more generally, may extend dramatically under these conditions. Therefore, the low-field monitoring of reactivity on time scales which may approach tens of minutes could become a future reality.

ASSOCIATED CONTENT

Supporting Information

Kinetic fitting of reaction rates, example UV and NMR spectra, characterization data for **6**

AUTHOR INFORMATION

Corresponding Author

*Email for S. B. D.: simon.duckett@york.ac.uk

ORCID

Ben. J. Tickner 0000-0002-8144-5655
Peter J. Rayner 0000-0002-6577-4117
Simon B. Duckett 0000-0002-9788-6615

Notes

The authors declare no competing financial interests.

ACKNOWLEDGMENTS

Financial support from the Wellcome Trust (Grants 092506 and 098335), the MRC (MR/M008991/1), the EPSRC (B.J.T. studentship) and the University of York is gratefully acknowledged.

REFERENCES

(1) Hunger, M.; Weitkamp, J. *Angew. Chem.* **2001**, *40*, 2954-2971.
(2) Nikolaou, P.; Goodson, B. M.; Chekmenev, E. Y. *Chem. Eur. J.* **2015**, *21*, 3156-3166.
(3) Zeng, H.; Lee, Y.; Hilty, C. *Anal. Chem.* **2010**, *82*, 8897-8902.
(4) Jannin, S.; Helm, L.; Bodenhausen, G. *J. Am. Chem. Soc.* **2010**, *132*, 5006-5007.
(5) Keshari, K. R.; Wilson, D. M. *Chem. Soc. Rev.* **2014**, *43*, 1627-1659.
(6) Nelson, S. J.; Kurhanewicz, J.; Vigneron, D. B.; Larson, P. E. Z.; Harzstark, A. L.; Ferrone, M.; van Criekinge, M.; Chang, J. W.; Bok, R.; Park, I.; Reed, G.; Carvajal, L.; Small, E. J.; Munster, P.; Weinberg, V. K.; Ardenkjaer-Larsen, J. H.; Chen, A. P.; Hurd, R. E.; Odegardstuen, L.-I.; Robb, F. J., et al. *Sci. Transl. Med.* **2013**, *5*, 198ra108.
(7) Eisenschmid, T. C.; Kirss, R. U.; Deutsch, P. P.; Hommeltoft, S. I.; Eisenberg, R.; Bargon, J.; Lawler, R. G.; Balch, A. L. *J. Am. Chem. Soc.* **1987**, *109*, 8089-8091.
(8) Bowers, C. R.; Weitekamp, D. P. *J. Am. Chem. Soc.* **1987**, *109*, 5541-5542.
(9) Hövener, J. B.; Pravdivtsev, A. N.; Kidd, B.; Bowers, C. R.; Glöggler, S.; Kovtunov, K. V.; Plaumann, M.; Katz-Brull, R.; Buckenmaier, K.; Jerschow, A. *Angew. Chem.* **2018**, *57*, 11140-11162.
(10) Tickner, B. J.; Parker, R. R.; Whitwood, A. C.; Duckett, S. B. *Organomet.* **2019**, *38*, 4377-4382.
(11) Kiryutin, A. S.; Sauer, G.; Yurkovskaya, A. V.; Limbach, H.-H.; Ivanov, K. L.; Buntkowsky, G. *J. Phys. Chem. C.* **2017**, *121*, 9879-9888.
(12) Ahlquist, M.; Gustafsson, M.; Karlsson, M.; Thaning, M.; Axelsson, O.; Wendt, O. F. *Inorg. Chim. Acta* **2007**, *360*, 1621-1627.
(13) Sellies, L.; Reile, I.; Aspers, R.; Feiters, M. C.; Rutjes, F. P. J. T.; Tessari, M. *Chem. Commun.* **2019**, 55, 7235-7238.
(14) Bhattacharya, P.; Chekmenev, E. Y.; Perman, W. H.; Harris, K. C.; Lin, A. P.; Norton, V. A.; Tan, C. T.; Ross, B. D.; Weitekamp, D. P. *J. Magn. Reson.* **2007**, *186*, 150-155.
(15) Cavallari, E.; Carrera, C.; Di Matteo, G.; Bondar, O.; Aime, S.; Reineri, F. *Front. Oncol.* **2020**, *10*, 497.
(16) Wang, W.; Xu, J.; Zhao, Y.; Qi, G.; Wang, Q.; Wang, C.; Li, J.; Deng, F. *Phys. Chem. Chem. Phys.* **2017**, *19*, 9349-9353.
(17) Kovtunov, K. V.; Zhivonitko, V. V.; Corma, A.; Koptyug, I. V. *J. Phys. Chem. Lett.* **2010**, *1*, 1705-1708.
(18) Svyatova, A.; Kononenko, E. S.; Kovtunov, K. V.; Lebedev, D.; Gerasimov, E. Y.; Bukhtiyarov, A.; Prosvirin, I.;

Bukhtiyarov, V.; Müller, C. R.; Fedorov, A. *Cat. Sci. Technol.* **2020**, *10*, 99-104.
(19) Zhivonitko, V. V.; Sorochkina, K.; Chernichenko, K.; Kótai, B.; Földes, T.; Pápai, I.; Telkki, V.-V.; Repo, T.; Koptyug, I. *Phys. Chem. Chem. Phys.* **2016**, *18*, 27784-27795.
(20) Sorochkina, K.; Zhivonitko, V. V.; Chernichenko, K.; Telkki, V.-V.; Repo, T.; Koptyug, I. V. *J. Phys. Chem. Lett.* **2018**, *9*, 903-907.
(21) Permin, A. B.; Eisenberg, R. *J. Am. Chem. Soc.* **2002**, *124*, 12406-12407.
(22) Godard, C.; Duckett, S. B.; Polas, S.; Tooze, R.; Whitwood, A. C. *J. Am. Chem. Soc.* **2005**, *127*, 4994-4995.
(23) Adams, R. W.; Aguilar, J. A.; Atkinson, K. D.; Cowley, M. J.; Elliott, P. I. P.; Duckett, S. B.; Green, G. G. R.; Khazal, I. G.; Lopez-Serrano, J.; Williamson, D. C. *Science* **2009**, *323*, 1708-1711.
(24) Ivanov, K. L.; Pravdivtsev, A. N.; Yurkovskaya, A. V.; Vieth, H.-M.; Kaptein, R. *Prog. Nucl. Magn. Reson.* **2014**, *81*, 1-36.
(25) Rayner, P. J.; Burns, M. J.; Olaru, A. M.; Norcott, P.; Fekete, M.; Green, G. G. R.; Highton, L. A. R.; Mewis, R. E.; Duckett, S. B. *Proc. Natl. Acad. Sci.* **2017**, *114*, E3188-E3194.
(26) Dücker, E. B.; Kuhn, L. T.; Münnemann, K.; Griesinger, C. *J. Magn. Reson.* **2012**, *214*, 159-165.
(27) Theis, T.; Ortiz, G. X.; Logan, A. W.; Claytor, K. E.; Feng, Y.; Huhn, W. P.; Blum, V.; Malcolmson, S. J.; Chekmenev, E. Y.; Wang, Q.; Warren, W. *Sci. Adv.* **2016**, *2*, e1501438.
(28) Shen, K.; Logan, A. W. J.; Colell, J. F. P.; Bae, J.; Ortiz Jr, G. X.; Theis, T.; Warren, W. S.; Malcolmson, S. J.; Wang, Q. *Angew. Chem.* **2017**, *129*, 12280-12284.
(29) Zhang, G.; Colell, J. F. P.; Glachet, T.; Lindale, J. R.; Reboul, V.; Theis, T.; Warren, W. S. *Angew. Chem.* **2019**, *131*, 11235-11241.
(30) Mewis, R. E.; Green, R. A.; Cockett, M. C. R.; Cowley, M. J.; Duckett, S. B.; Green, G. G. R.; John, R. O.; Rayner, P. J.; Williamson, D. C. *J. Phys. Chem. B* **2015**, *119*, 1416-1424.
(31) Iali, W.; Rayner, P. J.; Alshehri, A.; Holmes, A. J.; Ruddlesden, A. J.; Duckett, S. B. *Chem. Sci.* **2018**, *9*, 3677-3684.
(32) Barskiy, D. A.; Knecht, S.; Yurkovskaya, A. V.; Ivanov, K. L. *Prog. Nucl. Magn. Reson.* **2019**.
(33) Theis, T.; Truong, M. L.; Coffey, A. M.; Shchepin, R. V.; Waddell, K. W.; Shi, F.; Goodson, B. M.; Warren, W. S.; Chekmenev, E. Y. *J. Am. Chem. Soc.* **2015**, *137*, 1404-1407.
(34) Barskiy, D. A.; Shchepin, R. V.; Tanner, C. P. N.; Colell, J. F. P.; Goodson, B. M.; Theis, T.; Warren, W. S.; Chekmenev, E. Y. *ChemPhysChem* **2017**, *18*, 1493-1498.
(35) Semenova, O.; Richardson, P. M.; Parrott, A. J.; Nordon, A.; Halse, M. E.; Duckett, S. B. *Anal. Chem.* **2019**, *91*, 6695-6701.
(36) Rayner, P. J.; Tickner, B. J.; Iali, W.; Fekete, M.; Robinson, A. D.; Duckett, S. B. *Chem. Sci.* **2019**, *10*, 7709-7717.
(37) Iali, W.; Rayner, P. J.; Duckett, S. B. *Sci. Adv.* **2018**, *4*, eaao6250.
(38) Rayner, P. J.; Richardson, P. M.; Duckett, S. B. *Angew. Chem.* **2020**, *132*, 2732-2736.
(39) Tickner, B. J.; Iali, W.; Roy, S. S.; Whitwood, A. C.; Duckett, S. B. *ChemPhysChem* **2019**, *20*, 241-245.
(40) Iali, W.; Roy, S. S.; Tickner, B. J.; Ahwal, F.; Kennerley, A. J.; Duckett, S. B. *Angew. Chem.* **2019**, *131*, 10377-10381.
(41) Zhou, Z.; Yu, J.; Colell, J. F.; Laasner, R.; Logan, A. W.; Barskiy, D. A.; Shchepin, R. V.; Chekmenev, E. Y.; Blum, V.; Warren, W. S. *J. Phys. Chem. Lett.* **2017**, *8*, 3008-3014.
(42) Carravetta, M.; Johannessen, O. G.; Levitt, M. H. *Phys. Rev. Lett.* **2004**, *92*, 153003.
(43) Tickner, B. J.; Lewis, J. S.; John, R. O.; Whitwood, A. C.; Duckett, S. B. *Dalton Trans.* **2019**, *48*, 15198-15206.
(44) Tickner, B. J.; Semenova, O.; Iali, W.; Rayner, P. J.; Whitwood, A. C.; Duckett, S. B. *Cat. Sci. Technol.* **2020**, 1343-1355.
(45) Asmus, C.; Mozziconacci, O.; Schöneich, C. *J. Phys. Chem. A* **2015**, *119*, 966-977.
(46) Lopalco, A.; Dalwadi, G.; Niu, S.; Schowen, R. L.; Douglas, J.; Stella, V. J. *J. Pharm. Sci.* **2016**, *105*, 705-713.
(47) Melzer, E.; Schmidt, H.-L. *Biochem. J.* **1988**, *252*, 913-915.
(48) Leussing, D. L.; Hanna, E. M. *J. Am. Chem. Soc.* **1966**, *88*, 693-696.
(49) Vazquez-Serrano, L. D.; Owens, B. T.; Buriak, J. M. *Inorg. Chim. Acta* **2006**, *359*, 2786-2797.
(50) Richardson, P. M.; John, R. O.; Parrott, A. J.; Rayner, P. J.; Iali, W.; Nordon, A.; Halse, M. E.; Duckett, S. B. *Phys. Chem. Chem. Phys.* **2018**, *20*, 26362-26371.
(51) Mewis, R. E.; Fekete, M.; Green, G. R. R.; Whitwood, A. C.; Duckett, S. B. *Chem. Commun.* **2015**, *51*, 9857-9859.
(52) Margolis, S. A.; Coxon, B. *Anal. Chem.* **1986**, *58*, 2504-2510.
(53) Esposito, A.; Lukas, A.; Meany, J. E.; Pocker, Y. *Canad. J. Chem.* **1999**, *77*, 1108-1117.
(54) Griffith, E. C.; Carpenter, B. K.; Shoemaker, R. K.; Vaida, V. *Proc. Natl. Acad. Sci.* **2013**, *110*, 11714-11719.
(55) Tickner, B. J.; John, R. O.; Roy, S. S.; Hart, S.; Whitwood, A. C.; Duckett, S. B. *Chem. Sci.* **2019**, *10*, 5235-5245.
(56) Shchepin, R. V.; Birchall, J. R.; Chukanov, N. V.; Kovtunov, K. V.; Koptyug, I. V.; Theis, T.; Warren, W. S.; Gelovani, J. G.; Goodson, B. M.; Shokouhi, S. *Chem. Eur. J.* **2019**, *25*, 8829-8836.
(57) Barskiy, D. A.; Kovtunov, K. V.; Koptyug, I. V.; He, P.; Groome, K. A.; Best, Q. A.; Shi, F.; Goodson, B. M.; Shchepin, R. V.; Truong, M. L. *ChemPhysChem* **2014**, *15*, 4100-4107.
(58) Buckenmaier, K.; Rudolph, M.; Back, C.; Misztal, T.; Bommerich, U.; Fehling, P.; Koelle, D.; Kleiner, R.; Mayer, H. A.; Scheffler, K. *Sci. Rep.* **2017**, *7*, 1-9.
(59) Gong, Q.; Gordji-Nejad, A.; Blümich, B.; Appelt, S. *Anal. Chem.* **2010**, *82*, 7078-7082.